

Radio sky reveals primordial electron-proton interactions

Shyam Balaji,¹ Maura E. Ramírez-Quezada,² Céline Boehm³

For several decades, astronomers have measured the electromagnetic emission in the universe from the lowest to the highest energies with incredible precision. The lowest end of the spectrum, corresponding to radio waves, is fairly well studied and understood. Yet there is a long standing discrepancy between measurements and predictions, which has prompted the construction of many new models of radio emitters. Here we show that remnant electron-proton interactions, leading to photon production in the early universe, also referred to as cosmic free-free emission, solves the discrepancy between theory and observations. While the possibility of cosmic free-free emission has been postulated for several decades, this is the first time that the amplitude and shape of the signal has been computed and its existence demonstrated. Using current measurements we estimate this emission to become important from around a redshift of $z \simeq 2150$. This contribution from fundamental particles and interactions represents the lowest energy test from the early universe of one of the pillars of modern physics, Quantum Electrodynamics. The next generation of deep radio surveys will be able to measure primordial signals from this cosmic era with greater precision and further solidify our understanding of the radio sky.

At the lowest energy tail of the electromagnetic spectrum lies radio waves. These are emitted by a number of astrophysical objects such as active galactic nuclei, radio galaxies, star forming galaxies, as well as any sources capable of producing high energy charged particles moving through diffuse galactic and inter-galactic magnetic fields¹². This radio background has been the

subject of intense study since its discovery and imaged over large areas of the sky and at multiple frequencies^{10,35}. At frequencies above the radio spectrum, lies the cosmic microwave background (CMB). Since its discovery in 1965 by Wilson and Penzias, the latter has been studied in great detail. Analyses of its angular spectrum support the existence of both dark matter, dark energy (or the so-called cosmological constant), the notion of a hot big-bang and inflation. Early measurements of the CMB by the COBE experiment indicated that the CMB obeys a near perfect black-body spectrum; a conclusion that has remained robust for forty years¹. The physics of the CMB has continued to develop, now testing both the standard model of cosmology to a higher degree of precision and constraining new physics that can manifest as deviations from current theoretical expectations. In addition, a qualitatively new cosmological probe, the physics of 21 cm HI emission/absorption at the end of the so-called Dark Ages and beginning of the comic dawn have emerged with implication in the radio domain.

As such, it may seem that the study of cosmic electromagnetic emission in the radio-microwave range is largely completed. Yet, deviations of the CMB spectrum have been predicted^{34,38} and possibilities of new physics manifesting as a deviation in the Rayleigh tail^{19,20,37} have been proposed. Space-based experiments such as PIXIE³¹ have been planned to measure these possible deviations and will be critical to determine whether the CMB is indeed a perfect black-body spectrum.¹ Furthermore, there is a noticeable discrepancy between naive extension of the CMB blackbody to low frequency and observations of radio frequencies between 10^7 - 10^9 Hz, which deserves to be

¹The ARCADE experiments^{5,6} did in fact claim to find hints of deviation at a few GHz but the results have since been strongly challenged⁷.

investigated and is the subject of this work.

Such a discrepancy could be due to large foreground contributions, which subsequent models have tried to address²¹ or the presence of new physics, such as dark matter decay or late-time dark matter annihilation, primordial black holes or cosmic strings^{19,20,41}. Although they could also originate from other late time processes such as reionisation, structure formation or magnetic fields^{39,40}. Studying the $10^7 - 10^9$ Hz regime is thus critical to refine our understanding of modern cosmology.

The most well-known and studied model to explain this discrepancy, PB96, was developed by Protheroe and Biermann¹⁸. In order to estimate the extragalactic radio background down to frequencies of kHz, the PB96 model takes into account contributions from normal galaxies (NG) and radio galaxies (RG). The normal galaxies contribution is larger than that of radio galaxies in the lower frequency regime 10^3 - 10^6 Hz while the radio galaxies emission dominates in the 10^6 - 10^9 Hz range. However, despite its success in explaining the RG background, PB96 cannot reproduce the total radio background emission that has been observed in the 10^7 - 10^9 Hz regime. Other, more recent models of the CRB²¹, modulate extragalactic contributions within a larger parameter region in an attempt to match source counts.

Here we provide a more economical solution by showing that an additional radio source of primordial origin can explain the difference between the PB96 model and the observed radio background, and we quantify its magnitude for the first time. This contribution arises from the bremsstrahlung emission associated with electron-proton elastic scattering interactions for a very

specific range of redshifts. This process is supposed to cease as the number of free electrons and protons get sufficiently suppressed. In the chronology of the cosmos, this important phase is termed “recombination” due to the universe cooling and electrons and protons combining to form neutral Hydrogen atoms. During the recombination epoch, existing CMB photons decouple from matter at $z \simeq 1090^2$. However during this period, the free electrons and protons continue to scatter through QED interactions and emit low frequency bremsstrahlung photons.

These photons constitute a different population from the CMB as they are not part of the thermal bath. Their energy corresponds to the radio range as they get redshifted and diluted by cosmic expansion. This same band of photons can also be efficiently absorbed by the same interaction in reverse. Here we show however that for a very specific range of redshifts, the bremsstrahlung photons emitted by this free-free emission are not completely absorbed by the reverse process. As a result, many of these photons from primordial origins contribute to the radio background today. More surprisingly even, this small contribution can fit the radio discrepancy between theory and diffuse radio flux measurements precisely⁸.

Calculating the number of photons emitted and absorbed by electron-proton interactions

Recombination, is one of the most important phases in the history of the universe. Since it is not instantaneous, free protons and electrons can continue to interact and produce low energy photons through the radiative process $e + p \rightarrow e + p + \gamma$. As the photon energy reduces, the probability of emission increases. In light of this, one expects this process to be theoretically infrared (IR)

divergent, predicting production of an infinite number of photons. A result that is clearly not physical. We will see in subsequent sections that within the context of Quantum Field Theory (QFT) such an IR divergence is cancelled by the reverse process, ensuring that only a finite number of photons can be observed. Hence the study of such a channel provides, in principle, a remarkable window into QED at low energy and where the IR cancellation takes place. Furthermore, we will see that the bremsstrahlung photons considered are spectrally separated from the usual CMB photons. Therefore, they do not thermalise into the same blackbody spectrum and can persist as a distinct non-thermal population in the present universe's radio sky.

To determine the fate of these emitted photons, one needs to solve a set of coupled Boltzmann equations to follow the evolution of the energy distributions of electron, proton and photon wherein both the $e + p \rightarrow e + p + \gamma$ and $e + p + \gamma \rightarrow e + p$ processes should be included. However, since the focus of this letter is on photons and ordinary matter is meant to be fully thermalised during recombination, it suffices to compute the evolution of the photon distribution. For details, please refer to Sec. 1 in Methods.

The subtlety in such a calculation, is to accurately describe the population of photons that could be reabsorbed by the reverse process. To do this, we first compute the differential number of photons of energy E_γ produced by free-free emission $\frac{\partial^2 n_{\text{ems}}}{\partial z \partial E_\gamma}$, and remove the photons through the absorption term $\frac{\partial^2 \tilde{n}_{\text{abs}}}{\partial z \partial E_\gamma}$. Considering that electrons and protons follow a Maxwell-Boltzmann distribution, these two quantities are given by

$$\frac{\partial^2 n_{\text{ems}}}{\partial z \partial E_\gamma} = \frac{\partial Q_{\text{ems}}}{\partial E_\gamma} \mathcal{J}(z), \quad \frac{\partial^2 \tilde{n}_{\text{abs}}}{\partial z \partial E_\gamma} = \frac{\partial Q_{\text{abs}}}{\partial E_\gamma} \mathcal{J}(z), \quad (1)$$

where n_γ refers to the net photon density and the Jacobian factor $\mathcal{J}(z) = \frac{1+z}{T} \left| \frac{dt}{dz} \right|$. The rates $\frac{\partial Q_{\text{ems}}}{\partial E_\gamma}$ and $\frac{\partial Q_{\text{abs}}}{\partial E_\gamma}$ are the results of phase space integrals which are given in Eqs. (16) and (20) respectively.

We define

$$\frac{\partial^2 n_{\text{abs}}}{\partial z \partial E_\gamma} = f_\gamma(E_\gamma) \frac{\partial^2 \tilde{n}_{\text{abs}}}{\partial z \partial E_\gamma}, \quad \text{with } f_\gamma(E_\gamma) = \frac{\pi^2}{((1+z)E_\gamma)^2} \frac{\partial n_\gamma}{\partial E_\gamma}, \quad (2)$$

where f_γ is the non-thermal photon distribution function related to the net photon emission number density. Since we are interested in the evolution of the number density of photons emitted over time, we have expressed the photon number density in terms of the redshift z . This is achieved by using the relationship between the proper time t and z ^{14,17} with matter and dark energy densities of $\Omega_M = 0.265$ ^{15,16} and $\Omega_\Lambda = 0.685$ ¹⁵ respectively.

Eventually the number of photons that are expected to contribute to the radio background is given by the balance of these two terms. The integro-partial differential equation describing the net observable photon number density is given by

$$\frac{\partial^2 n_\gamma}{\partial z \partial E_\gamma} = \left[\frac{\partial^2 n_{\text{ems}}}{\partial z \partial E_\gamma} - f_\gamma(E_\gamma) \frac{\partial^2 \tilde{n}_{\text{abs}}}{\partial z \partial E_\gamma} \right] a(z)^3, \quad (3)$$

with boundary condition $\frac{\partial n}{\partial E_\gamma}(z_{\text{neq}}) = 0$, where z_{neq} is the redshift at which the free-free photons begin to accumulate as a distinct non-thermal population. The first term on the right handside corresponds to photon injection while the second corresponds to absorption. The necessary physical condition that absorption can never exceed emission is ensured dynamically by f_γ . Finally, we have taken into account the expansion of the universe by introducing the cosmic scale factor $a(z)$ for dilution. We then solve Eq. (3) to obtain $\frac{\partial n}{\partial E_\gamma}$ as a function of redshift z .

Predicting the radio background associated with $ep \rightarrow ep\gamma$

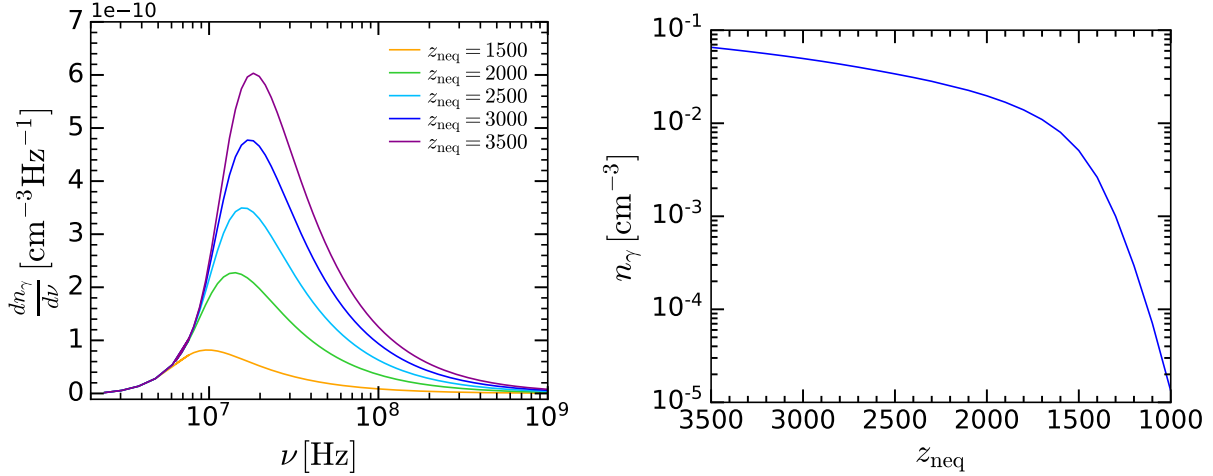


Figure 1: Differential photon number density as a function of frequency at present time $z = 0$ (left panel). Each colour corresponds to different decoupling times varying from $z_{\text{neq}} = 3500$ (purple line) to $z_{\text{neq}} = 1500$ (orange line). The free-free photon number density at present time, is shown as a function of the decoupling redshift z_{neq} (right panel).

The number density of photons expected today as a result of the emission and absorption process after recombination is plotted in Fig. 1 as a function of frequency (left panel) and out-of-equilibrium redshift z_{neq} (right panel). The fact that n_γ is significant (at most $\mathcal{O}(10^{-1}) \text{ cm}^{-3}$) indicates that the emission rate dominates over the absorption rate at radio frequencies which manifests in the radio background estimated in this letter. The differential number density peaks somewhere between 10^7 - 10^8 Hz but more importantly, we note that it becomes negligible for frequencies below 10^7 Hz. This is a very important result. In fact, theoretically, the number of photons emitted at extreme low frequencies is expected to diverge to infinity, but this occurs for absorption as well. Using QFT, we are able to demonstrate that both contributions actually cancel out each other at

frequencies smaller than 10^7 Hz due to f_γ . Furthermore for $z_{\text{neq}} \simeq 1000$, the expected number density falls down to $\mathcal{O}(10^{-5}) \text{ cm}^{-3}$. This is unsurprising given the rapid reduction in electrons and protons forming neutral hydrogen during recombination. Hence, we observe three distinct regimes. At frequencies greater than 10^{10} Hz, the number of bremsstrahlung photons emitted by free-free interactions is negligible. In the 10^7 - 10^{10} Hz range, both the emission and absorption increase but the emission is greater than the absorption. Finally for frequencies smaller than 10^7 Hz, both the emission and absorption terms diverge but they also cancel each other out. These regimes in conjunction leads to a finite result in a definite radio frequency range. Measurement of this signal should enable precise determination of when the free-free photons in the universe left thermal equilibrium, and ultimately should allow robust constraints to be placed on z_{neq} .

We note that classical estimates of a possible radio contribution were mentioned in early studies of the CMB^{28,30}. However this contribution was deemed negligible at frequencies greater than a few GHz, where the CMB signal is dominant²⁹. Furthermore, at the time, radio sources in the foreground were modelled poorly, which explains why this contribution has been forgotten until now. Finally, it is worth mentioning that classical free-free interaction estimates are plagued by divergent IR behaviour which is in turn also regulated with arbitrary cutoff scales^{32,33}. As such the classical approach is sufficient for crude estimates of the magnitude of the effect, but it doesn't provide a precise physical spectrum, particularly at low frequency. Using a full QFT treatment has enabled us to solve this issue and, as a result, we provide the first estimate of the radio background emitted by bremsstrahlung emission associated with cosmic free-free interactions.²

²We have disregarded other process such as e - e and p - p bremsstrahlung as they are greatly suppressed due to

Relevance of this novel radio background for current observations

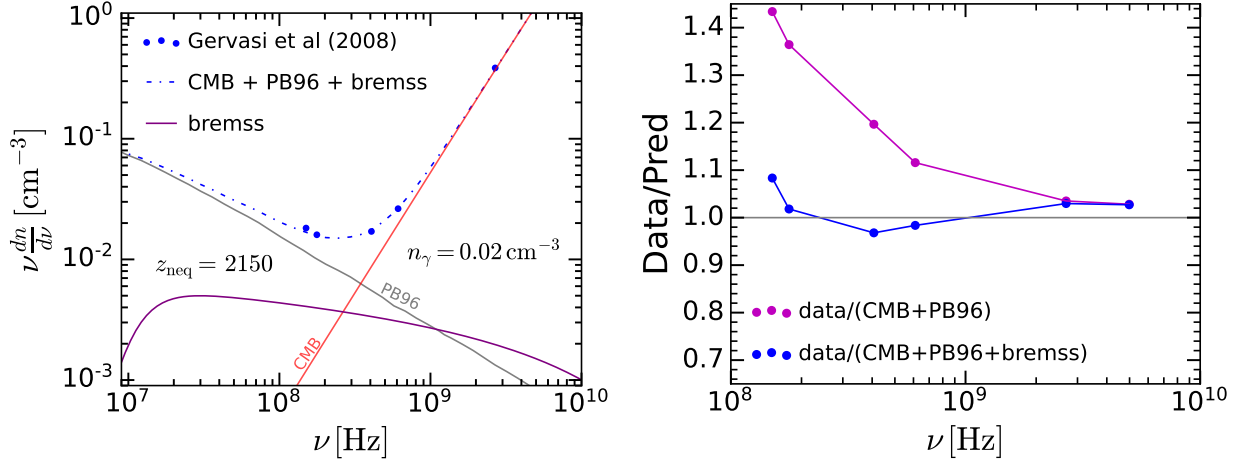


Figure 2: Left panel: Differential photon number density by frequency vs frequency. We show the total theoretical prediction (blue dashed line) and data⁸ (blue points). We also show PB96 foreground model (gray line), the CMB blackbody (red line) and recombination bremsstrahlung decoupling at $z_{\text{neq}} = 2150$ (purple line). Right panel: The ratio between data⁸ and the prediction with (blue) and without (magenta) the recombination bremsstrahlung contribution.

To understand the relevance of this background, we introduce foreground models and radio observations. We shall use the PB96 model¹⁸, as it is the most well-known and studied that intends to explain the CRB foreground. In order to estimate the radio foreground down to frequencies of kHz the PB96 model takes into account contributions from normal and radio galaxies. The model also includes free-free emission and absorption by the warm and hot ionized components of the interstellar medium and by synchrotron self-absorption.

⁸In the left panel of Fig. 2, we show that the cosmic free-free contribution considered in this having the same mass.

work can resolve the tension observed between PB96 and radio source count⁸. The CMB black-body is shown in red and is computed using Eq. (14) of ¹¹ while PB96 predictions of galactic foregrounds are shown in gray. The free-free contribution discussed in this work is shown in purple and the sum of all relevant contributions is shown in blue dot-dashed. Inspecting the right panel of Fig. 2, we see the ratio between model predictions and data can exceed 43%. We find that if free-free photons start manifesting as a separate population from CMB photons from $z_{\text{neq}} \simeq 2150$, we can reduce the tension with data to at most 8%. The number density in the present universe corresponding to this is $n_\gamma = 0.024 \text{ cm}^{-3}$, which is very small relative to the CMB number density of approximately 411 cm^{-3} , but still represents around 5% of the radio foreground contribution considered. The result also provides a definite prediction for the expected radio spectrum between the frequencies of the observed source counts in the range $10^7 < \nu < 10^9 \text{ Hz}$ which will be tested at high precision by the Square Kilometre Array and the Expanded Very Long Array in the near future. As explained above, frequencies below 10^7 Hz receive negligible correction from free-free contributions and therefore no significant excess radio signal from this process is expected in this region.

Conclusion

We have shown that the bremsstrahlung emission associated with free-free electron-proton scattering in the early universe constituted a significant source of radio emission today and explains the discrepancy between models of radio sources and observations.

Numerical estimates of the photon net number density indicate that if free-free photons decoupled from the thermal bath at $z_{\text{neq}} \approx 2150$, the tension between observational data in ⁸ and the theoretical predictions can be significantly reduced, from 43%, 36%, 19% and 11% to 8%, 1%, 4% and 2% at frequencies of 151 MHz, 178 MHz, 408 MHz and 610 MHz respectively. The photon number density at present time for this signal is $n_\gamma \simeq 0.02 \text{ cm}^{-3}$, which is very suppressed compared to that of the CMB but not insignificant relative to the radio sky. Finally we see that frequencies below 10^7 Hz and above 10^{10} Hz receive negligible corrections from recombination bremsstrahlung and hence, no significant excess radio signal from this process is expected in these regions. Therefore, our work provides a robust test of QED from recombination in the universe down to temperatures of about 0.1 eV. The Square Kilometre Array and Expanded Very Long Array are expected to probe intermediate frequencies with high resolution which would further strengthen our understanding of this process. Finally, discovery of potential nano-Jansky populations and radio relics from clusters as additional sources of faint diffuse emission will enable more precise data driven extraction of z_{neq} in the future.

1. Mather, J. & Others Measurement of the Cosmic Microwave Background spectrum by the COBE FIRAS instrument. *Astrophys. J.* **420** pp. 439-444 (1994)
2. Hinshaw, G. & Others Nine-Year Wilkinson Microwave Anisotropy Probe (WMAP) Observations: Cosmological Parameter Results. *Astrophys. J. Suppl.* **208** pp. 19 (2013)
3. Bennett, C. & Others Nine-Year Wilkinson Microwave Anisotropy Probe (WMAP) Observations: Final Maps and Results. *Astrophys. J. Suppl.* **208** pp. 20 (2013)

4. Ade, P. & Others Planck 2015 results. XIII. Cosmological parameters. Astron. Astrophys. **594** pp. A13 (2016)
5. Fixsen, D., Kogut, A., Levin, S., Limon, M., Lubin, P., Mirel, P., Seiffert, M. & Wollack, E. The Temperature of the CMB at 10-GHz. Astrophys. J. **612** pp. 86-95 (2004)
6. Fixsen, D. & Others ARCADE 2 Measurement of the Extra-Galactic Sky Temperature at 3-90 GHz. Astrophys. J. **734** pp. 5 (2011)
7. Subrahmanyan, R. & Cowsik, R. Is there an Unaccounted for Excess in the Extragalactic Cosmic Radio Background?. Astrophys. J. **776** pp. 42 (2013)
8. Gervasi, M., Tartari, A., Zannoni, M., Boella, G. & Sironi, G. The contribution of the Unresolved Extragalactic Radio Sources to the Brightness Temperature of the sky. Astrophys. J. **682** pp. 223 (2008)
9. Condon, J. Radio Emission from Normal Galaxies. Annual Review Of Astronomy And Astrophysics. **30**, 575-611 (1992),
10. Oliveira-Costa, A., Tegmark, M., Gaensler, B., Jonas, J., Landecker, T. & Reich, P. A model of diffuse Galactic Radio Emission from 10 MHz to 100 GHz. Mon. Not. Roy. Astron. Soc. **388** pp. 247 (2008)
11. Hill, R., Masui, K. & Scott, D. The Spectrum of the Universe. Appl. Spectrosc. **72**, 663-688 (2018)

12. Singal, J., Stawarz, Ł., Lawrence, A. & Petrosian, V. Sources of the radio background considered. Monthly Notices Of The Royal Astronomical Society. **409**, 1172-1182 (2010,9), <https://doi.org/10.1111>
13. Carmeli, M., Hartnett, J. & Oliveira, F. The Cosmic time in terms of the redshift. Found. Phys. Lett. **19** pp. 277-283 (2006)
14. Macdonald, A. Comment on ‘The Cosmic time in terms of the redshift’, by Carmeli et al. Found. Phys. Lett. **19** pp. 631-632 (2006)
15. Aghanim, N. & Others Planck 2018 results. VI. Cosmological parameters. Astron. Astrophys. **641** pp. A6 (2020), [Erratum: Astron. Astrophys. 652, C4 (2021)]
16. Scott, D. & Smoot, G. Cosmic background radiation mini-review. (2004,6)
17. Condon, J. & Matthews, A. Λ CDM Cosmology for Astronomers. Publ. Astron. Soc. Pac. **130**, 073001 (2018)
18. Protheroe, R. & Biermann, P. A New estimate of the extragalactic radio background and implications for ultrahigh-energy gamma-ray propagation. Astropart. Phys. **6** pp. 45-54 (1996), [Erratum: Astropart. Phys. 7, 181 (1997)]
19. Pospelov, M., Pradler, J., Ruderman, J. & Urbano, A. Room for New Physics in the Rayleigh-Jeans Tail of the Cosmic Microwave Background. Phys. Rev. Lett. **121**, 031103 (2018)
20. Ghara, R., Mellema, G. & Zaroubi, S. Astrophysical information from the Rayleigh-Jeans Tail of the CMB. JCAP. **3**, 055 (2022)

21. Nițu, I., Bevins, H., Bray, J. & Scaife, A. An updated estimate of the cosmic radio background and implications for ultra-high-energy photon propagation. Astropart. Phys. **126** pp. 102532 (2021)
22. Hoare, M., Kurtz, S., Lizano, S., Keto, E. & Hofner, P. Ultra-Compact H II Regions and the Early Lives of Massive Stars. (2006,3)
23. Beckert, T., Duschl, W. & Mezger, P. Free-free and recombination radiation from massive star-forming regions. Astronomy And Astrophysics. **356** pp. 1149-1156 (2000,4)
24. Cooray, A. & Furlanetto, S. Free - free emission at low radio frequencies. Astrophys. J. Lett. **606** pp. L5-L8 (2004)
25. Oh, S. Observational signatures of the first luminous objects. The Astrophysical Journal. **527**, 16 (1999)
26. Oh, S. & Mack, K. Foregrounds for 21cm observations of neutral gas at high redshift. Mon. Not. Roy. Astron. Soc. **346** pp. 871 (2003)
27. Loeb, A. Contribution of Bremsstrahlung Emission from Ly α Clouds to the Microwave Background Fluctuations. The Astrophysical Journal. **459**, L5 (1996)
28. Zeldovich, Y. & Sunyaev, R. The Interaction of Matter and Radiation in a Hot-Model Universe. Astrophys. Space Sci., **4**, 301-316 (1969,7)
29. Hu, W. & Silk, J. Thermalization and spectral distortions of the cosmic background radiation. Phys. Rev. D. **48**, 485-502 (1993,7), <https://link.aps.org/doi/10.1103/PhysRevD.48.485>

30. Chan, K. & Jones, B. Distortions of the 3 K background radiation spectrum: observational constraints on the early thermal history of the universe. *Astrophys. J.* . **195** pp. 1-11 (1975,1)
31. Kogut, A. & Others The Primordial Inflation Explorer (PIXIE): A Nulling Polarimeter for Cosmic Microwave Background Observations. *JCAP.* **7** pp. 025 (2011)
32. Brussaard, P. & Hulst, H. Approximation Formulas for Nonrelativistic Bremsstrahlung and Average Gaunt Factors for a Maxwellian Electron Gas. *Rev. Mod. Phys.*. **34**, 507-520 (1962,7), <https://link.aps.org/doi/10.1103/RevModPhys.34.507>
33. Chluba, J., Ravenni, A. & Bolliet, B. Improved calculations of electron–ion bremsstrahlung Gaunt factors for astrophysical applications. *Mon. Not. Roy. Astron. Soc.*. **492**, 177-194 (2020)
34. Silk, J. Cosmic black body radiation and galaxy formation. *Astrophys. J.*. **151** pp. 459-471 (1968)
35. Clark, T., Brown, L. & Alexander, J. Spectrum of the Extra-galactic Background Radiation at Low Radio Frequencies. *Nature.* . **228**, 847-849 (1970,11)
36. Dent, J., Ferrer, F. & Krauss, L. Constraints on Light Hidden Sector Gauge Bosons from Supernova Cooling. (2012,1)
37. Chluba, J. Tests of the CMB temperature–redshift relation, CMB spectral distortions and why adiabatic photon production is hard. *Mon. Not. Roy. Astron. Soc.*. **443**, 1881-1888 (2014)
38. Chluba, J. & Sunyaev, R. The evolution of CMB spectral distortions in the early Universe. *Mon. Not. Roy. Astron. Soc.*. **419** pp. 1294-1314 (2012)

39. Reis, I., Fialkov, A. & Barkana, R. High-redshift radio galaxies: a potential new source of 21-cm fluctuations. Mon. Not. Roy. Astron. Soc. **499**, 5993-6008 (2020)
40. Vernstrom, T., Heald, G., Vazza, F., Galvin, T., West, J., Locatelli, N., Fornengo, N. & Pinetti, E. Discovery of magnetic fields along stacked cosmic filaments as revealed by radio and X-ray emission. Mon. Not. Roy. Astron. Soc. **505**, 4178-4196 (2021)
41. Diamanti, R., Lopez-Honorez, L., Mena, O., Palomares-Ruiz, S. & Vincent, A. Constraining Dark Matter Late-Time Energy Injection: Decays and P-Wave Annihilations. JCAP. **2** pp. 017 (2014)

Correspondence Correspondence and requests for materials should be addressed to S. Balaji (email: sbalaji@lpthe.jussieu.fr).

Statement of contribution The idea was proposed by C. Boehm. S. Balaji derived the solution for the dynamic number density. M.E. Ramirez-Quezada produced all the displayed plots. S. Balaji and M.E. Ramirez-Quezada identified the dominant channel and performed all calculations and analysis. All authors have contributed to all stages of the project and the writing of the manuscript.

Acknowledgements We would like to thank Anastasia Fialkov and Matthew Johnson for helpful discussions at the beginning of the project. We would also like to thank Ravi Subrahmanyan for useful discussions regarding radio source counts. CB and MRQ would like to thank the Perimeter Institute for their hospitality when the project started and CB would like to thank Laurent Freidel for stimulating discussions on QFT at low energy. SB is supported by funding from the European Union’s Horizon 2020 research and innovation programme under grant agreement No 101002846 (ERC CoG “CosmoChart”) as well as support from the

Initiative Physique des Infinis (IPI), a research training program of the Idex SUPER at Sorbonne Université.

MRQ is supported by JSPS KAKENHI Grant Number 20H01897.

Author Information ¹*Laboratoire de Physique Théorique et Hautes Energies (LPTHE), UMR 7589
CNRS & Sorbonne Université, 4 Place Jussieu, F-75252, Paris, France*

²*Department of Physics, University of Tokyo, Bunkyo-ku, Tokyo 113–0033, Japan*

³*School of Physics, The University of Sydney, NSW 2006, Australia*

Conflicts of interest The authors declare that they have no competing financial interests.

List of Figures

- 1 Differential photon number density as a function of frequency at present time $z = 0$ (left panel). Each colour corresponds to different decoupling times varying from $z_{\text{neq}} = 3500$ (purple line) to $z_{\text{neq}} = 1500$ (orange line). The free-free photon number density at present time, is shown as a function of the decoupling redshift z_{neq} (right panel). 7

- 2 Left panel: Differential photon number density by frequency vs frequency. We show the total theoretical prediction (blue dashed line) and data⁸ (blue points). We also show PB96 foreground model (gray line), the CMB blackbody (red line) and recombination bremsstrahlung decoupling at $z_{\text{neq}} = 2150$ (purple line). Right panel: The ratio between data⁸ and the prediction with (blue) and without (magenta) the recombination bremsstrahlung contribution. 9

Methods

1 Emission rate computation

We compute the rate of bremsstrahlung emission in electron-proton scattering $e(p_1) + p(p_2) \rightarrow e(p_3) + p(p_4) + \gamma(k)$. The photon emission rate Q_{ems} from this process is generically given by³⁶,

$$Q_{\text{ems}} = d\Pi_\gamma \int d\Pi_1 d\Pi_2 d\Pi_3 d\Pi_4 \mathcal{S} |\mathcal{M}_\gamma|^2 \delta^4(p_1 + p_2 - p_3 - p_4 - k) f_1 f_2 (1 - f_3) (1 - f_4) \quad (4)$$

where, $|\mathcal{M}_\gamma|^2$ is the squared amplitude for bremsstrahlung emission, the symmetry factor $\mathcal{S} = 1$ for e - p scattering, $d\Pi_j = d^3\mathbf{p}_j / (2E_j(2\pi)^3)$ are the particle phase space factors and f_j denotes the distribution function of the particles involved in the process. In the low energy limit and ignoring Pauli blocking, we take $(1 - f_{3,4}) \rightarrow 1$ as well as $E_{1,3} = m_e$ and $E_{2,4} = m_p$. Since the photon abundance is small compared to the particles in the thermal plasma, we can neglect f_γ in Q_{ems} . For non-relativistic particles, the distribution function for electrons and protons is Maxwell-Boltzmann

$$f(p_j) = \frac{n_j}{2} \left(\frac{2\pi}{m_j T} \right)^{3/2} e^{-\mathbf{p}_j^2/2m_j T}, \quad (5)$$

where n_j and m_j are the number density and mass of the particles in the process. Finally, the squared amplitude of free-free emission ($ep \rightarrow ep\gamma$) is given by,

$$\sum_{\text{spins}} |\mathcal{M}_\gamma|^2 = e^2 \sum_{\text{spin}} |\mathcal{M}_0|^2 \left[\frac{p_3}{p_3 \cdot k} - \frac{p_1}{p_1 \cdot k} \right]^2, \quad (6)$$

where \mathcal{M}_0 corresponds to e - p scattering. The total expression in terms of variables u and v , defined in Eq. (9), is therefore given by,

$$\begin{aligned} \sum_{\text{spins}} |\mathcal{M}_\gamma|^2 = & \frac{2e^6}{m_e^2 \mu T^3 x^2 (u+v - 2z\sqrt{uv})} \left[(m_e^2 + m_p^2 + 2\mu T(u+v))^2 - 4\mu^2 T^2 (u-v)^2 \right. \\ & \left. + (m_e^2 + m_p^2 + \mu T(2z\sqrt{uv} + u+v))^2 - 2\mu T(m_e^2 + m_p^2)(-2z\sqrt{uv} + u+v) \right] \quad (7) \end{aligned}$$

In order to compute the emission rate we make the useful change of variables $l = p_2 - p_3$, $r = p_2 - p_4$ ³⁶. Taking the photon soft limit, for these parameters leads to

$$\begin{aligned} \mathbf{r}^2 &= \mu T(u+v - 2y\sqrt{uv}), \\ \mathbf{l}^2 &= \mu T(u+v + 2y\sqrt{uv}), \\ \mathbf{r} \cdot \mathbf{l} &= \mu T(u-v), \end{aligned} \quad (8)$$

where the reduced mass is given by $\mu \equiv \frac{2m_p m_e}{m_e + m_p}$. The new variables y , u and v are dimensionless and are defined in terms of the temperature by

$$y = \cos \theta, \quad u = \frac{\mathbf{p}_i^2}{\mu T}, \quad v = \frac{\mathbf{p}_f^2}{\mu T}. \quad (9)$$

which corresponds to the angle θ between the initial (\mathbf{p}_i) and final (\mathbf{p}_f) 3-momentum of the particles in the centre of momentum coordinates,

$$\mathbf{p}_{1,2} = \mathbf{P} \pm \mathbf{p}_i, \quad \mathbf{p}_{3,4} = \mathbf{P}' \pm \mathbf{p}_f. \quad (10)$$

From here, we rewrite the product of the distribution functions $f_1 f_2$ in Eq. (4) as

$$f_1 f_2 \rightarrow \exp \left[-\frac{\mathbf{P}^2}{\mu T} - \frac{\mathbf{p}_i^2}{\mu T} - \left(\frac{1}{m_e T} - \frac{1}{m_p T} \right) \mathbf{P} \cdot \mathbf{p}_i \right]. \quad (11)$$

We may then rewrite the integration variables in Eq. (4) in terms of 3-momentum integrals over \mathbf{p}_i , \mathbf{P} and \mathbf{p}_f which can then be written as integrals in terms of the dimensionless u , v and y like

$$\int d^3 \mathbf{p}_f = \pi (\mu T)^{3/2} \int \sqrt{v} dv \int_{-1}^1 dy, \quad (12)$$

$$\int d^3 \mathbf{P} f_1 f_2 = \frac{\pi (\mu T)^{3/2}}{m_p^2} f(u), \quad (13)$$

$$\int d^3 \mathbf{p}_i = 4\pi \int p_i^2 d\mathbf{p}_i = 2\pi (\mu T)^{3/2} \int \sqrt{u} du \quad (14)$$

where $f(u)$ is obtained after integration by replacing the definitions in Eq. (9) into Eq. (11), the explicit expression is given by

$$f(u) = \left[2e^{-u} m_p \sqrt{u} (\mu - m_p) + e^{\frac{u\mu(\mu - 2m_p)}{m_p^2}} \sqrt{\pi} (m_p^2 (1 + 2u) - u(4m_p - 2\mu)\mu) \operatorname{erfc} \left(\frac{\sqrt{u}(\mu - m_p)}{m_p} \right) \right] \quad (15)$$

where erfc is the complimentary error function. Finally the differential photon emission rate is

$$\frac{\partial Q_{\text{ems}}}{\partial x} = \frac{\alpha_{em}^3 \mu^{7/2} n_p n_e}{4\pi (m_e m_p)^{11/2} \sqrt{T} x} \int du dv dy \delta(u - v - x) \sqrt{uv} f(u) \mathcal{I}(u, v, y) \quad (16)$$

where n_e and n_p are the electron and proton number densities respectively and $x = E_\gamma(1 + z)/T$, where we define E_γ at redshift $z = 0$ and x at arbitrary z . Notice that we have integrated over \mathbf{p}_4 already. The function $\mathcal{I}(u, v, y)$ is related to the squared amplitude for bremsstrahlung in terms of variables u and v ,

$$\mathcal{I}(u, v, y) = \frac{1}{(u+v - 2y\sqrt{uv})} \left[(m_e^2 + m_p^2 + 2\mu T(u+v))^2 + (m_e^2 + m_p^2 + \mu T(2y\sqrt{uv} + u+v))^2 - 2\mu T(m_e^2 + m_p^2)(-2y\sqrt{uv} + u+v) - 4\mu^2 T^2(u-v)^2 \right]. \quad (17)$$

We use the delta function to integrate over v leading to the replacement $v \rightarrow u - x$.

2 Absorption rate computation

We compute photon absorption rate in electron-proton scattering $e(p_1) + p(p_2) + \gamma(k) \rightarrow e(p_3) + p(p_4)$. The differential photon absorption rate is calculated in a very similar fashion to the emission rate. Notice that for the case of photon absorption ($ep\gamma \rightarrow ep$), we can directly compute the squared scattering amplitude for the inverse process by replacing $k \rightarrow -k$

$$\sum_{\text{spins}} |\mathcal{M}_\gamma(k)|^2 = \sum_{\text{spins}} |\mathcal{M}'_\gamma(-k)|^2 \quad (18)$$

leading to

$$\sum_{\text{spins}} |\mathcal{M}'_\gamma|^2 = e^2 \sum_{\text{spin}} |\mathcal{M}_0|^2 \left[\frac{p_1}{p_1 \cdot k} - \frac{p_3}{p_3 \cdot k} \right]^2. \quad (19)$$

where \mathcal{M}'_γ is the amplitude for absorption, which takes a similar form as the amplitude for the emission process.

Recasting with the same dimensionless variables as before, we define the differential photon absorption rate by³⁶

$$\frac{\partial Q_{\text{abs}}}{\partial x} = \frac{\alpha_{em}^3 \mu^{7/2} n_p n_e}{4\pi (m_e m_p)^{11/2} \sqrt{T} x} \int dudvdy \delta(u - v + x) \sqrt{uv} \mathcal{I}(u, v, y) f(u). \quad (20)$$

Finally, the expression for the \mathcal{I} function in the emission and absorption rates is given by Eq. (17).

The delta function in the absorption rate leads to the replacement of $u \rightarrow v - x$.